N-Rich Silicon Nitride Angled-MMI for coarse wavelength division (de)multiplexing in the O-band

THALÍA DOMÍNGUEZ BUCIO[1,*], ALI Z. KHOKHAR[1], GORAN Z. MASHANOVICH[1], AND FREDERIC Y. GARDES[1]

[1] Optoelectronics Research Centre, University of Southampton, Southampton SO17 1BJ, UK
[*] Corresponding author: tdb2g12@soton.ac.uk

Compiled January 8, 2018

We report the design and fabrication of a compact angled multimode interferometer (AMMI) on a 600nm thick N-rich silicon nitride platform (n=1.92) optimised to match the International Telecommunication Union (ITU) coarse wavelength division (de)multiplexing (CWDM) standard in the O telecommunication band. The demonstrated device exhibited a good spectral response with $\Delta\lambda$=20nm, BW_{3dB} ∼11nm, IL<1.5dB and XT∼20dB. Additionally, it showed a high tolerance to dimensional errors <120pm/nm and low sensitivity to temperature variations <20pm/°C, respectively. This device had a fooprint of 0.02x1.7mm^2 with the advantage of a simple design and a back-end-of-line compatible fabrication process that enables multilayer integration schemes due to its processing temperature <400°C.

OCIS codes: (130.0130) Integrated optics; (130.3120) Integrated optics devices; (130.7408) Wavelength filtering devices.

http://dx.doi.org/10.1364/ao.XX.XXXXXX

1. INTRODUCTION

Wavelength division (de)multiplexing devices (WDM) capable of splitting/combining the light into/from multiple wavelengths are components required for a wide variety of photonic applications, particularly to increase the capacity of high-speed telecommunication photonic integrated circuits. WDM devices demonstrated in literature include arrayed waveguide gratings, planar concave gratings and micro-ring resonators [1–3].

All these devices have been realised in a variety of platforms, including silica and silicon-on-insulator (SOI), which pose different challenges that must be overcome to achieve competitive performances. On one hand, the low-index contrast silica platform has allowed fabricating devices with low insertion losses (IL) and low cross-talk (XT) at expense of increased footprints. On the other hand, devices on the SOI platform tend to be compact but they exhibit higher losses and a higher sensitivity to both dimensional and temperature variations. To address this situation, Hu et al. proposed angled-multimode interferometer (AMMI) (de)multiplexers based on multimode dispersive waveguides capable of providing low IL with a high tolerance to fabrication errors [4]. Nevertheless, SOI AMMIs are still prone to a low tolerance to temperature variations due to the large thermo-optic coefficient of Si ∼1.8x10^{-4}/°C.

Under this context, the silicon nitride (SiN) platform has proven to be a good compromise between footprint and spectral performance that enables the fabrication of WDM devices with low IL and a high tolerance to temperature changes [5–7]. In a previous paper, we demonstrated that stoichiometric SiN with a thickness of 300nm and a refractive index ∼2.0 can be used to fabricate AMMIs with a high tolerance to temperature changes using a relatively simple fabrication process [8]. Nonetheless, regardless of their low sensitivity to temperature variations, they exhibited IL and XT values close to the ones typically observed in the SOI platform.

We propose using a recently demonstrated N-rich SiN platform with a refractive index of 1.92 to improve the performance of AMMI structures in the O telecommunication band (1260-1320nm) [9]. This material not only has the potential to reduce the XT and IL of the devices, but it can also decrease their footprint as lower refractive indices tend to translate into shorter device lengths. In addition, it has processing temperatures <400°C that make its fabrication process compatible with back-end-of-line (BEOL) integration and, thus, it can potentially be used for multilayer integration schemes. In this letter, we report the design, fabrication and characterisation of a 4-channel AMMI optimised to match the first 4 channels of the ITU CWDM standard G.694.2 using a 600nm thick N-rich SiN platform. We discuss the spectral characteristics of the device and the effect that both temperature and dimensional variations have on its central wavelengths.

2. DESIGN AND FABRICATION

The basic structure of an AMMI consist of a multimode dispersive waveguide of width W_{MDW} with input/output waveguides of width W_{IO}. The input/output waveguides are tilted at an angle θ_t and tapered from their single-mode width to W_a before entering the multimode waveguide as illustrated in fig. 1. The input/output waveguides are placed along the multimode

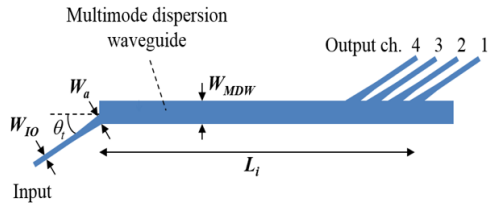

Fig. 1. Schematic diagram of the 4-channel AMMI (de)multiplexer.

region to satisfy the inverted self-imaging condition described by Hu et al. [4]. This arrangement allows splitting the input signal into multiple wavelengths that are imaged at different axial positions (L_i) respect to the input waveguide. These axial positions can be estimated using equation 1 which depends on the effective index of the fundamental mode in the multimode waveguide (n_{eff}) and the wavelength of the ith output channel (λ_i) [10].

$$L_i = \frac{4n_{eff}W_{MDW}^2}{\lambda_i} \quad (1)$$

The maximum channel count (N_{max}) and the minimum channel spacing ($\Delta\lambda_{min}$) of the AMMI device are limited by equation 2 and 3, where x_min is the minimum separation between adjacent output waveguides required for a minimal cross-coupling.

$$N_{max} < \frac{2W_{MDW}cos\theta_t}{W_a} \quad (2)$$

$$\Delta\lambda_{min} > \frac{W_a + x_{min}}{4n_{eff}sin\theta_t}\left(\frac{\lambda_i}{W_{MDW}}\right)^2 \quad (3)$$

These analytical equations were used to explored the design space to simplify the optimisation process. In this case, equation 1 was used to set W_{MDW} to 18μm as it is the highest value that allows maintaining the overall length of the device well below 2mm. This total length ensures that the footprint of the device is comparable to that of other WDM devices demonstrated on the SiN platform. Then, equations 2 and 3 were used to determine the range of W_a and θ_t values that would provide the desired channel count of 4 and the channel spacing ($\Delta\lambda$) of 20nm. The selected W_{MDW} and the estimated ranges were carefully explored using *FIMMWAVE* to optimise the structural parameters of the device to provide spectral responses with a 3dB bandwidth (BW_{3dB}) of 10nm, insertion losses (IL)<1dB and cross-talk (XT) between 15 and 20dB. Table 1 summarises the optimised parameters for the 4-channel AMMI (de)multiplexer obtained from the simulations when using a refractive index of 1.92 for the N-rich SiN. The design was finalised by simulating separately the taper section used to convert W_{IO}= 750nm into W_a=7.5μm to determine its length of 300μm.

Table 1. Optimised design parameters for the 4-channel AMMI.

$W_a = 7.5\mu m, W_{MDW} = 18\mu m, \theta_t = 0.3rad$				
λ_i $[nm]$	1271	1291	1311	1331
L_i $[\mu m]$	1609	1581	1555	1528

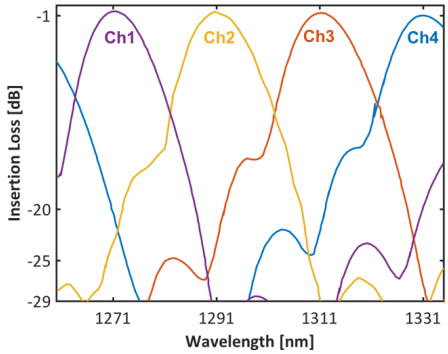

Fig. 2. Simulated spectral response for the 4-channel AMMI with optimised parameters $\theta_t = 0.3rad$, $W_a = 7.5\mu m$ and $W_{MDW} = 18\mu m$.

Figure 2 illustrates the spectral response simulated for the AMMI (de)multiplexer with the optimised parameters that exhibits IL<1dB, BW_{3dB}=10nm and XT<20dB which meet the requirements originally set for the design.

The layout used to characterise the spectral response of the device included an array of with W_{MDW} variations of $\pm$20 and $\pm$40nm to study their sensitivity to dimensional variations. All the AMMI structures had a grating coupler consisting of a single-mode waveguide tapered up to a 10μm surface grating with a period of 950nm as a means to couple light in the O-band. It is important to mention that a separate structure with two tapered grating couplers connected back-to-back was also fabricated for normalisation purposes.

The structures were fabricated on a 6" Si wafer with a 2μm thermally-grown SiO_2 layer and a 600nm N-rich SiN film deposited at 350°C using a NH_3 PECVD process detailed in [9]. The layout was defined on the wafers using electron beam lithography with a high-resolution 850nm ZEP520A resist. The design was then transferred onto the N-rich SiN layer using ICP etching with an etch depth of 600nm using a SF_6:CHF_3 chemistry. A 1μm thick layer of PECVD SiO_2 was finally deposited at 350°C on top of the devices as cladding. Figure 3 shows microscopic images of the fabricated AMMI devices.

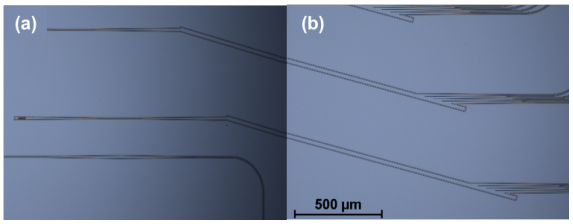

Fig. 3. Microscopic images of the fabricated AMMI at the (a) input waveguides and (b) output waveguides.

The spectral response of the device was characterised using an Agilent 8164B tunable laser source with a wavelength tuning range between 1260-1360nm. The polarisation of the light was controlled to ensure that only TE modes could propagate on the structures. Additionally, the temperature of the measurements was controlled with a thermal stage to study the effect of the temperature on the spectral response of the devices.

3. RESULTS AND DISCUSSION

Figure 4 shows the measured spectral response of the fabricated AMMI for TE polarisation. The oscillations present in the spectra are the combined result of the Fabry-Perot effect produced by the presence of the grating couplers and the polarization state of the measurement set-up. Regardless of these oscillations, it can be observed that the experimental result is in good agreement with the simulation. The channel spacing matches closely the required 20nm specification with$\Delta\lambda$=19.9$\pm$0.5nm and the central wavelength of all the channels only deviates by <1nm from the desired λ_i. The BW_{3dB} for all the channels is ~11.0$\pm$0.4nm which is well within the initial specifications and covers almost 55% of the total $\Delta\lambda$. In addition, the mean IL after normalising the spectrum to that of the grating couplers with losses of 14dB/grating is estimated to be ~ 1.3dB with a maximum non-uniformity of 0.4dB across the channels. Finally, the mean XT between adjacent channels is ~21dB with a maximum XT non-uniformity of 11dB. This strong XT non-uniformity is produced by the difference in the free spectral range (FSR) of the channels. In this case, Ch4 has a FSR of only ~68nm which limits the XT of Ch1 to values <16dB, while Ch1 has a larger FSR ~94nm which reduces the XT of Ch4 to values <27dB. The overall XT of the device could be reduced <30dB by increasing the W_{MDW} to reduce the $\Delta\lambda_{min}$ or by reducing W_a to increase N_{max}. However, either solution will come at a expense of increased device footprint or higher IL, respectively.

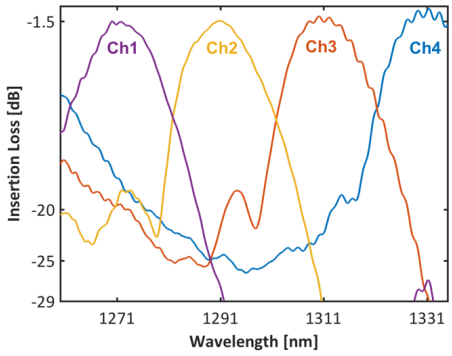

Fig. 4. Spectral response of the demonstrated 4-channel AMMI on the N-rich SiN platform measured at 20°C.

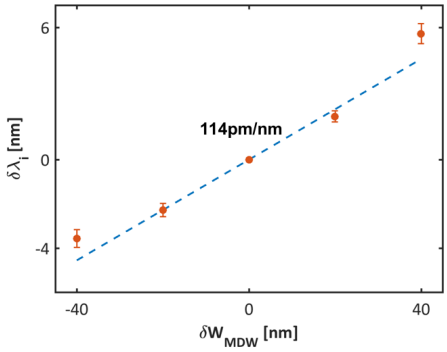

Fig. 5. Sensitivity of the spectral shift as a function of the fabrication error in the width of the AMMI multimode waveguide observed in the O-band.

Figure 5 presents the sensitivity of the spectral shift ($\delta\lambda_i$) respect to the fabrication error in the width of the multimode waveguide (δW_{MDW}). This result reveals that the AMMI exhibits an almost linear sensitivity of 114pm/nm, which is consistent with the values observed in SOI AMMIs [11]. This value is almost one order of magnitude lower than the sensitivity exhibited by other SOI WDM devices. This improved tolerance can be attributed to the negligible shift experience by the n_{eff} of the multimode waveguide with fabrication errors due to its increased dimensions compared to single-mode waveguides.

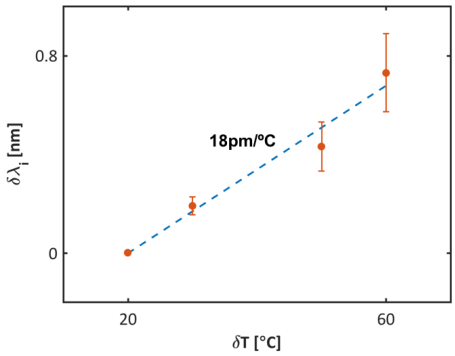

Fig. 6. Sensitivity of the spectral shift as a function of temperature variations exhibited by the AMMI in the O-band.

The $\delta\lambda_i$ as a function of the temperature variation δT is illustrated in fig. 6. In this case, it can be observed that $\delta\lambda_i$ is directly proportional to the temperature variation with a sensitivity of 18pm/°C. This sensitivity can be described as a function of the thermally induced changes on the n_{eff} of the AMMI structure ($\delta n_{eff}/\delta T$) using equation 4 [10]. This last value can be directly linked to the thermo-optic coefficient of the SiN layer ($\delta n_{SiN}/\delta T$) using equation 5, where $\delta n_{SiO_2}/\delta T$ is the thermo-optic coefficient of the SiO_2 cladding, $\delta n_{eff}/\delta n_{SiN}$ the sensitivity of the n_{eff} of the multimode waveguide to n_{SiN}, and $\delta n_{eff}/\delta n_{SiO_2}$ the n_{eff} sensitivity to n_{SiO_2}.

$$\frac{\delta\lambda_i}{\delta T} = \frac{\lambda_i}{n_{eff}}\frac{\delta n_{eff}}{\delta T} \tag{4}$$

$$\frac{\delta n_{eff}}{\delta T} = \frac{\delta n_{eff}}{\delta n_{SiN}}\frac{\delta n_{SiN}}{\delta T} + \frac{\delta n_{eff}}{\delta n_{SiO_2}}\frac{\delta n_{SiO_2}}{\delta T} \tag{5}$$

These two equations were used to estimate the thermo-optic coefficient of the N-rich SiN layer using $\delta n_{SiO_2}/\delta T$=0.95x10^{-5} [12] after extracting $\delta n_{eff}/\delta n_{SiN}$=0.98 and $\delta n_{eff}/\delta n_{SiO_2}$=0.11 from simulations. The computed results reveal that the N-rich layers with a n=1.92 have a thermo-optic coefficient ~ 2.2x10^{-5} which is similar to the values reported for other SiN platforms in the literature [12].

Table 2 compares the characteristics of the N-rich SiN AMMI with other CWDM devices available in the literature. It can be observed that the performance of the AMMI in terms of XT and IL is comparable to other published devices, such as arrayed waveguide gratings (AWG) and planar concave gratings (PCG) on SOI and SiN. Furthermore, its XT is closer to values ~40dB exhibited by silica AWGs [14]. In terms of footprint, the proposed AMMI is larger than SOI devices which are in the order of μm^2, but it still maintains the higher tolerance to dimensional and temperature variations characteristic of SiN devices with a more compact design than that of silica devices.

Table 2. Summary of the characteristics of WDM devices operating in the near-infrared including footprint, channel spacing, insertion losses (IL), cross-talk (XT), sensitivity to dimensional variations and sensitivity to temperature. The footprint of all the devices is calculated without taking into account the access waveguides.

Device	Footprint [mm^2]	Channels/ Spacing [nm]	IL [dB]	XT [dB]	$\delta\lambda/\delta W$ [pm/nm]	$\delta\lambda/\delta T$ [pm/°C]
Silica PCG [13]	18 x 17	48 x 0.8	<4	35	-	
Silica AWG [14]	-	16 x 0.8	3.2	30	-	12
SOI PCG [15, 16]	0.650 x 0.15	4 x 20	2.0 - 3.5	∼20	-	-
SOI AWG [3, 17]	0.310 x 0.26	4 x 20	1.6 - 5.0	∼20	∼1000	∼80
SOI AMMI [4]	0.012 x 1.21	4 x 21	2.0	20	100	-
SiN PCG [7]	-	16 x 0.2	1.5	30	-	-
SiN AWG [18]	0.600 x 1.80	8 x 1.6	1.5	24	-	11
This Work	0.020 x 1.70	4 x 19	<1.5dB	16 - 27	114	18

One of the major limitations of the AMMI is its reduce channel count, which makes it hardly scalable to dense WDM application where AWGs and PCGs offer a better performance. Furthermore, the proposed structure is polarisation dependent whereas silica AWGs present an almost polarisation independent operation. However, the 600nm thickness of the N-rich layer offers the possibility of fabricating polarisation independent AMMIs, as it is possible to design waveguides with the same effective index for both polarisations by carefully selecting their width. Still, the independent operation of the devices must be studied further as the width of the multimode waveguide required for polarisation independence may limit the amount of channels and the channel spacing supported by the structure.

4. CONCLUSIONS

We have demonstrated a 4-channel AMMI (de)multiplexer for CWDM with $\Delta\lambda$=20nm, BW_{3dB} ∼11nm, IL<1.5dB and XT<20dB. This performance is comparable to the state-of-the-art in SOI and SiN CWDM devices. Nevertheless, the AMMI structure allows taking advantage of the higher tolerance of SiN to fabrication and temperature variations with a with a more compact design than typical AWGs and PCGs devised for SiN. In addition, the low processing temperature of the N-rich layer makes this device compatible with multilayer CMOS BEOL integration. As a result, the demonstrated AMMI is an ideal candidate for commercial CWDM applications that require compactness with stability to temperature changes.

FUNDING

H2020 European Research Council (688516); Engineering and Physical Sciences Research Council (EPSRC) (EP/L021129/1, EP/N013247/1).

AKNOWLEDGMENTS

The authors acknowledge the financial support from the above listed funding bodies. The fabrication was carried out at the Southampton Nanofabrication Centre, University of Southampton, UK. All data supporting this study are openly available from the University of Southampton repository at

REFERENCES

1. W. Bogaerts, S. K. Selvaraja, P. Dumon, J. Brouckaert, K. D. Vos, D. V. Thourhout, and R. Baets, IEEE J. Sel. Top. Quantum Electron. **16**, 33 (2010).
2. J. Teng, P. Dumon, W. Bogaerts, H. Zhang, X. Jian, X. Han, M. Zhao, G. Morthier, and R. Baets, Opt. Express **17**, 14627 (2009).
3. S. Pathak, P. Dumon, D. Van Thourhout, and W. Bogaerts, IEEE Photonics J. **6**, 1 (2014).
4. Y. Hu, R. Jenkins, and F. Y. Gardes, Opt. Lett. **36**, 4488 (2011).
5. M. Piels, J. F. Bauters, M. L. Davenport, M. J. R. Heck, and J. E. Bowers, J. Light. Technol. **32**, 817 (2014).
6. D. Dai, Z. Wang, J. F. Bauters, M.-C. Tien, M. J. R. Heck, D. J. Blumenthal, and J. E. Bowers, Opt. Express **19**, 14130 (2011).
7. E. Ryckeboer, X. Nie, A. Z. Subramanian, D. Martens, P. Bienstman, S. Clemmen, S. Severi, R. Jansen, G. Roelkens, and R. Baets, Proc. SPIE **9891**, 98911K (2016).
8. T. Domínguez Bucio, A. Z. Khokhar, G. Z. Mashanovich, and F. Y. Gardes, Opt. Express **25**, 27310 (2017).
9. T. Domínguez Bucio, A. Z. Khokhar, C. Lacava, S. Stankovic, G. Z. Mashanovich, P. Petropoulos, and F. Y. Gardes, J. Phys. D. Appl. Phys. **50**, 025106 (2017).
10. Y. Hu, T. Li, D. J. Thomson, X. Chen, J. S. Penades, a. Z. Khokhar, C. J. Mitchell, G. T. Reed, and G. Z. Mashanovich, Opt. Lett. **39**, 1406 (2014).
11. Y. Hu, F. Y. Gardes, D. J. Thomson, G. Z. Mashanovich, and G. T. Reed, Appl. Phys. Lett. **102**, 7 (2013).
12. A. Arbabi and L. L. Goddard, Opt. Lett. **38**, 3878 (2013).
13. S. Janz, A. Balakrishnan, S. Charbonneau, P. Cheben, M. Cloutier, A. Delâge, K. Dossou, L. Erickson, M. Gao, P. A. Krug, B. Lamontagne, M. Packirisamy, M. Pearson, and D. X. Xu, IEEE Photonics Technol. Lett. **16**, 503 (2004).
14. A. Kaneko, S. Kamei, Y. Inoue, H. Takahashi, and A. Sugita, Electron. Lett. **36**, 318 (2000).
15. J. Brouckaert, G. Roelkens, S. K. Selvaraja, W. Bogaerts, P. Dumon, S. Verstuyft, D. Van Thourhout, and R. Baets, IEEE Photonics Technol. Lett. **21**, 1423 (2009).
16. J. F. Song, Q. Fang, T. Y. Liow, H. Cai, M. B. Yu, G. Q. Lo, and D.-L. Kwong, 2011 Opt. Fiber Commun. Conf. Expo. Natl. Fiber Opt. Eng. Conf. **1**, 1 (2011).
17. N. Juhari, P. S. Menon, A. A. Ehsan, and S. Shaari, "16-channel arrayed waveguide grating (AWG) demultiplexer design on SOI wafer for application in CWDM-PON," in "AIP Conference Proceedings," , vol. 9444 (2015), vol. 9444, pp. 944412–944412–6.
18. K. Shang, S. Pathak, C. Qin, and S. J. B. Yoo, IEEE Photonics J. **9**, 6601805 (2017).

REFERENCES

1. W. Bogaerts, S. K. Selvaraja, P. Dumon, J. Brouckaert, K. D. Vos, D. V. Thourhout, and R. Baets, "Silicon-on-Insulator Spectral Filters Fabricated With CMOS Technology," IEEE J. Sel. Top. Quantum Electron. **16**, 33–44 (2010).
2. J. Teng, P. Dumon, W. Bogaerts, H. Zhang, X. Jian, X. Han, M. Zhao, G. Morthier, and R. Baets, "Athermal Silicon-on-insulator ring resonators byoverlaying a polymer cladding on narrowedwaveguides," Opt. Express **17**, 14627–14633 (2009).
3. S. Pathak, P. Dumon, D. Van Thourhout, and W. Bogaerts, "Comparison of AWGs and Echelle Gratings for Wavelength Division Multiplexing on Silicon-on-Insulator," IEEE Photonics J. **6**, 1–9 (2014).
4. Y. Hu, R. Jenkins, and F. Y. Gardes, "Wavelength division (de) multiplexing based on dispersive self-imaging," Opt. Lett. **36**, 4488–4490 (2011).
5. M. Piels, J. F. Bauters, M. L. Davenport, M. J. R. Heck, and J. E. Bowers, "Low-Loss Silicon Nitride AWG Demultiplexer Heterogeneously Integrated With Hybrid III-V/Silicon Photodetectors," J. Light. Technol. **32**, 817–823 (2014).
6. D. Dai, Z. Wang, J. F. Bauters, M.-C. Tien, M. J. R. Heck, D. J. Blumenthal, and J. E. Bowers, "Low-loss Si3N4 arrayed-waveguide grating (de)multiplexer using nano-core optical waveguides," Opt. Express **19**, 14130–14136 (2011).
7. E. Ryckeboer, X. Nie, A. Z. Subramanian, D. Martens, P. Bienstman, S. Clemmen, S. Severi, R. Jansen, G. Roelkens, and R. Baets, "CMOS-compatible silicon nitride spectrometers for lab-on-a-chip spectral sensing," Proc. SPIE **9891**, 98911K–98911K–9 (2016).
8. T. Domínguez Bucio, A. Z. Khokhar, G. Z. Mashanovich, and F. Y. Gardes, "Athermal silicon nitride angled MMI wavelength division (de)multiplexers for the near-infrared," Opt. Express **25**, 27310–27320 (2017).
9. T. Domínguez Bucio, A. Z. Khokhar, C. Lacava, S. Stankovic, G. Z. Mashanovich, P. Petropoulos, and F. Y. Gardes, "Material and optical properties of low-temperature NH 3 -free PECVD SiN x layers for photonic applications," J. Phys. D. Appl. Phys. **50**, 025106 (2017).
10. Y. Hu, T. Li, D. J. Thomson, X. Chen, J. S. Penades, a. Z. Khokhar, C. J. Mitchell, G. T. Reed, and G. Z. Mashanovich, "Mid-infrared wavelength division (de)multiplexer using an interleaved angled multimode interferometer on the silicon-on-insulator platform." Opt. Lett. **39**, 1406–9 (2014).
11. Y. Hu, F. Y. Gardes, D. J. Thomson, G. Z. Mashanovich, and G. T. Reed, "Coarse wavelength division (de)multiplexer using an interleaved angled multimode interferometer structure," Appl. Phys. Lett. **102**, 7–11 (2013).
12. A. Arbabi and L. L. Goddard, "Measurements of the refractive indices and thermo-optic coefficients of Si3N4 and SiO(x) using microring resonances." Opt. Lett. **38**, 3878–81 (2013).
13. S. Janz, A. Balakrishnan, S. Charbonneau, P. Cheben, M. Cloutier, A. Delâge, K. Dossou, L. Erickson, M. Gao, P. A. Krug, B. Lamontagne, M. Packirisamy, M. Pearson, and D. X. Xu, "Planar Waveguide Echelle Gratings in Silica-On-Silicon," IEEE Photonics Technol. Lett. **16**, 503–505 (2004).
14. A. Kaneko, S. Kamei, Y. Inoue, H. Takahashi, and A. Sugita, "Athermal silica-based arrayed-waveguide grating (AWG) multi/demultiplexers with new low loss groove design," Electron. Lett. **36**, 318 (2000).
15. J. Brouckaert, G. Roelkens, S. K. Selvaraja, W. Bogaerts, P. Dumon, S. Verstuyft, D. Van Thourhout, and R. Baets, "Silicon-on-insulator CWDM power monitor/receiver with integrated thin-film InGaAs photodetectors," IEEE Photonics Technol. Lett. **21**, 1423–1425 (2009).
16. J. F. Song, Q. Fang, T. Y. Liow, H. Cai, M. B. Yu, G. Q. Lo, and D.-L. Kwong, "CWDM planar concave grating multiplexer/demultiplexer and application in ROADM," 2011 Opt. Fiber Commun. Conf. Expo. Natl. Fiber Opt. Eng. Conf. **1**, 1–3 (2011).
17. N. Juhari, P. S. Menon, A. A. Ehsan, and S. Shaari, "16-channel arrayed waveguide grating (AWG) demultiplexer design on SOI wafer for application in CWDM-PON," in "AIP Conference Proceedings," , vol. 9444 (2015), vol. 9444, pp. 944412–944412–6.
18. K. Shang, S. Pathak, C. Qin, and S.-J. Ben Yoo, "Low-loss compact silicon nitride arrayed waveguide gratings for photonic integrated circuits," IEEE Photon. J. **9**, 6601805 (2017).